frontiers in Energy Research

ORIGINAL RESEARCH
published: 11 January 2022
doi: 10.3389/fenrg.2021.794604

A Highly Efficient Graphene Gold Based Green Supercapacitor Coin Cell Device for Energy Storage

*Leonardo Vivas and Dinesh Pratap Singh**

Physics Department and Millennium Institute for Research in Optics (MIRO), Faculty of Science, University of Santiago of Chile (USACH), Santiago, Chile

Inclination to exploit renewable energy and their potential storage by facile, cost-effective, and above all in a green way are exactly what the current alternative energy research is looking for. The high-performance supercapacitor devices made up with the electrode materials synthesized in a simple and ecofriendly way are in utmost demand and the ultimate goal for widespread commercialization. Keeping these points in view, one pot green synthesis of active electrode material rGO-Au composite is achieved which not only performs as a very good supercapacitor in three-electrode configuration but also demonstrates extremely well as a coin cell device, ready to use. Ascorbic acid, which is commonly found in citrus fruits, plays an important role to reduce graphene oxide into rGO and simultaneously gold salt into gold nanoparticles, resulting in rGO-Au composite. The maximum recorded specific capacitance by CV measurement is 303.02 Fg^{-1} at a scan rate of 5 mVs^{-1}. Hindrance in the commercialization is caused by the differences in the supercapacitor performances between three electrode configurations and finally the proposed device. Here the proposed coin cell device exhibits maximum areal and mass specific capacitance of 62.43 $mFcm^{-2}$ and 56.09 Fg^{-1}, respectively, that is very high among all reported graphene based composite devices benefitted over with commercially viable high capacity retention up to 80% even after 10,000 cycles. The proposed device demonstrates high energy density (~ E_D = 7.79 Wh/Kg) comparable to batteries and an optimum power density (~ P_D = 2512.9 W/Kg) close to supercapacitor insinuating it is an effective green supercapacitor for commercialization.

Keywords: graphene, rGO-Au composites, green supercapacitors, ascorbic acid, coin cell device

OPEN ACCESS

Edited by:
Jiajun Wang,
Harbin Institute of Technology, China

Reviewed by:
Grzegorz Lota,
Poznań University of Technology, Poland
Hadi Hosseini,
Sharif University of Technology, Iran

****Correspondence:***
Dinesh Pratap Singh
dineshpsingh@gmail.com
orcid.org/0000-0002-2893-7749

Specialty section:
This article was submitted to Electrochemical Energy Conversion and Storage, a section of the journal Frontiers in Energy Research

Received: *13 October 2021*
Accepted: *02 December 2021*
Published: *11 January 2022*

Citation:
Vivas L and Singh DP (2022) A Highly Efficient Graphene Gold Based Green Supercapacitor Coin Cell Device for Energy Storage. Front. Energy Res. 9:794604. doi: 10.3389/fenrg.2021.794604

INTRODUCTION

Enormously increasing energy demands day by day and our huge dependency of daily life on it have motivated the researchers to think about alternative and sustainable energy resources to reduce the carbon emission, environmental pollution, and to address the global warming issue. The renewable energy sources are unlimited but with its own restrictions of availability such as the sun does not shine in the night and the wind will not blow as per our requirements. These limitations have enforced the researchers to store the energy in an efficient and ecofriendly way for the continuous uncut supply of day and night as per our demand. Electrochemical double layer capacitors, also known as supercapacitors, have gained much interest due to their fast charge/discharge rate, long operating life, and ability to achieve large specific capacitance (Kötz and Carlen, 2000; Aphale et al., 2015; Hosseini and Shahrokhian, 2018a; Hosseini and Shahrokhian, 2018b; Hosseini and

Shahrokhian, 2019). Owing to its excellent physical/chemical properties, carbon based materials are widely used as electrode materials in double-layer capacitors (Ramachandran et al., 2013; Azadfalah et al., 2021). Recently, among all materials graphene is in the forefront for use of electrode material in supercapacitors due to its astounding properties such as joint length of the C-C bond (~1.42 Å), highest specific surface area ~2630 m^2g^{-1} (single graphene sheet), unique optical properties with a band separation value of 0–0.25 eV, and very high electron mobility of 15,000 $cm^2 V^{-1} s^{-1}$ (Geim and Novoselov, 2007; Balandin et al., 2008; Zhang et al., 2009). Various methods were adopted for the synthesis of pristine and functionalized graphene for the electrode materials in supercapacitor. Du et al. (2010) synthesized two different types of functionalized graphene sheets by adopting low temperature thermal exfoliation method and studied their electrochemical performance. The one kind of functionalized graphene offered specific capacitance value of 230 Fg^{-1}, whereas the other showed the specific capacitance value ~100 Fg^{-1}. Similarly, a graphene-activated carbon composite, prepared by chemical activation method, demonstrated a specific capacitance of 122 g^{-1} while utilized as an electrode in a supercapacitor (Du et al., 2010; Ramachandran et al., 2013). Enhancement in the electrochemical performance of graphene was achieved by the decoration of nanoparticles on the surface (Ke and Wang, 2016). The graphene and its derivatives such as graphene oxides (GO) and functionalized graphene sheets, provide numerous benefits as a template for the homogenous distribution of metallic nanoparticles due to favorable interaction between nanoparticles and oxygen containing functional groups at the surface to achieve graphene nanoparticles hybrid structures. The large surface area is another benefit to make available a sufficient number of anchoring sites for the interaction and hence enhancement in desired properties (Khan et al., 2015; Ioni et al., 2016; Jokar et al., 2018). Due to its excellent electrical conductivity, biocompatibility, high surface to volume ratio, superior electrocatalytic/electrochemical activities, facile synthesis, and better control on structure and morphologies, the metallic nanoparticles including gold (Tommalieh et al., 2021), silver (Rodríguez-Otamendi et al., 2021), and copper (Das Jana et al., 2021) have attracted considerable interest as a suitable conductive dopant either *in situ* or *ex situ* (beyond the cost barrier) to enhance the electrochemical performances of electrode materials. Ultra-small Au nanoparticles were anchored on the NiO nanobelts by a two-step process of hydrothermal (160°C for 24 h) and ultrasonication and its electrochemical performance was studied by Tan et al. (2018). PMMA/r-GO/Au nanohybrids were achieved by first preparing PMMA latex and then by emulsion polymerization technique utilizing various chemicals such as potassium persulfate, hydrazine hydrate, and ammonium ferrous sulphate (Sahoo et al., 2017). Ma et al. (2019a) first synthesized carbon microspheres by the hydrothermal method at 220°C for 12 h further and porosity was achieved at ramp temperature of 450°C, 650°C, and 800°C for a defined time and finally the composite was achieved by sodium borohydride reduction of gold salt.

But its electrochemical properties have also been studied sparsely for the use of supercapacitor as an electrode material (Shabani Shayeh et al., 2015a; Li et al., 2016). The electrode PANI/rGO/AuNPs was prepared by utilizing a conductive polymer (PANI) as a binder to rGO decorated gold nanoparticles and cyclic voltammetry (CV) measurements resulted a specific capacitance of 303 Fg^{-1} and long cycle life.

Above all mentioned synthesis methods of rGO-Au composites demand very high temperature, a lengthy two-step process, or use of toxic chemicals/reducing agents. For example, thermal exfoliation of GO demands very high temperature of around 1000°C, whereas chemical exfoliation utilizes toxic chemicals such as hydrazine and ammonia. Furthermore, the composite formation was always achieved by the lengthy two-step method; first, synthesis of rGO by thermal or chemical exfoliation either at high temperature or utilizing toxic chemicals, second the composites were formed by the reduction of gold salt either by the hydrothermal method at high temperature, long time, or by reducing it with toxic chemicals or reagents.

Enhanced performances of the electrode materials or devices and above all ecofriendly and facile way of synthesis of composite, can always be counterpoised by the high cost of the gold salt. Furthermore, the gold salt is utilized as a first report for the synthesis of rGO-Au composite by *in situ* reduction with ascorbic acid which can be further extrapolated to various other metal salts such as silver and copper utilizing the same method (Chen et al., 2011; Yin et al., 2013).

In the current scenario, highly efficient energy storage devices, by utilizing electrode materials synthesized by a green approach are of great importance to address environmental issues. Keeping this as the utmost priority and without compromising with efficiency here we propose a very simple, facile, and *in-situ* decoration of Au nanoparticles on a graphene sheet. The simultaneous reduction of GO and gold salt is achieved in one step by a common reducing agent of ascorbic acid. This method not only reduced the use of toxic chemicals for the reduction of graphene oxide such as ammonia and hydrazine, but also overcame the requirement of an extra reagent for the reduction of gold salt. The use of ascorbic acid generally found in abundance in lots of fruits and vegetables have made the method greener and ecofriendly. The electrodes for the three-electrode configuration and coin cell device are prepared by the rGo/AuNPs nanocomposites with activated carbon and poly(methyl methacrylate) (PMMA) for supercapacitors. Moreover, the coin cell device utilizes very low-cost filter paper soaked into KOH solution as a separator in comparison to other separators used for various supercapacitors.

In summary we show the synthesis of rGO decorated with gold nanoparticles, which differs from other works by using a fast, low-cost, and environmentally friendly method that is the preamble to new syntheses with salts more economical than gold and that maintain the necessary performance for this type of device.

RESULTS AND DISCUSSION

The details of the synthesis of rGO-Au composites by reduction with ascorbic acid are described in detail in the experimental section and by A. Sina et al. (Abdolhosseinzadeh et al., 2015).

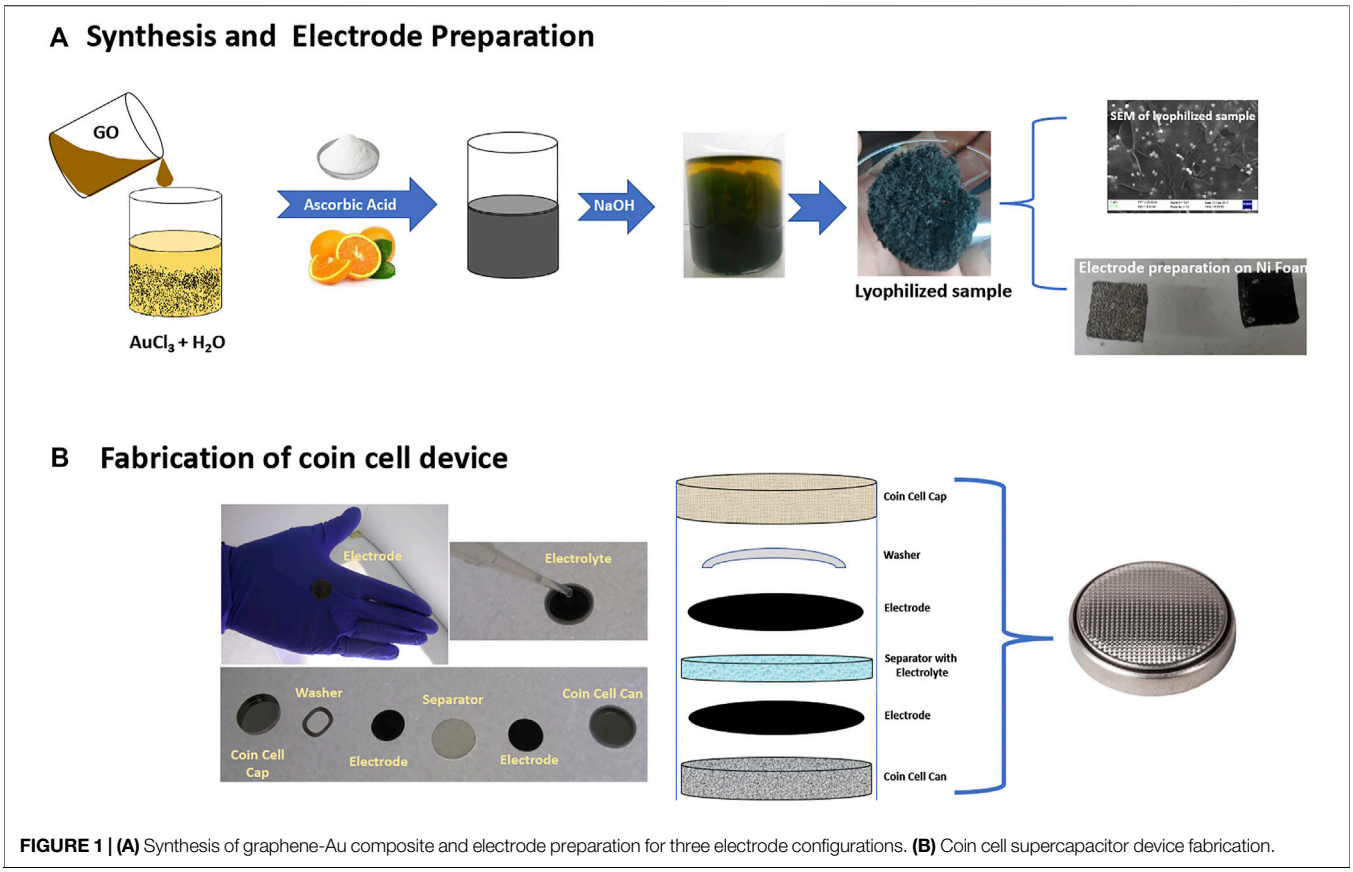

FIGURE 1 | (A) Synthesis of graphene-Au composite and electrode preparation for three electrode configurations. **(B)** Coin cell supercapacitor device fabrication.

Figures 1A,B are the details of the synthesis of composites, three electrode preparation, and fabrication of a coin cell device for various measurements.

Structural and Spectral Characterizations of the as Synthesized rGO-Au Nanocomposites

The structure of as synthesized rGO-Au nanocomposite was analyzed by XRD, Raman, and XPS spectra as shown in **Figure 2**. In **Figure 2A**, the diffraction peaks at angles 38.408°, 44.591°, 64.776°, and 77.708° correspond to (111), (200), (220), and (311) planes of Au nanoparticles, respectively, with a lattice parameter of a = 4.0640°A and space group Fm3m (ICDD No. 00-001-1174). Moreover, an additional peak observed at 2θ = 22.689° corresponds to a diffraction peak of reduced graphene oxide obtained with (002) set of graphitic planes (Janani et al., 2016). The XRD analysis confirms the formation of gold nanoparticles and the efficient reduction of graphene oxide into rGO by the reducing agent, ascorbic acid (Emiru and Ayele, 2017; Sze et al., 2017).

The recorded Raman spectra of the rGO-Au hybrid structure is shown in **Figure 2B**, which clearly reveals the main characteristic peaks of graphene such as G band (~1584 cm^{-1}) caused by the allowed E_{2g} mode at Γ point of the Brillouin zone (BZ) arises from Sp^2 hybridized C-C bond stretching. The second characteristic peak located at ~2699 cm^{-1} is also known as a 2D peak is a result of a second order two phonon process from the $A_1^{'}$ phonon in the BZ corner of the K point (Ferrari et al., 2006) and strongly dependent to the number of graphene layers and excitation wavelength of the laser light. Disorder induced, D and D + D′ peaks located at ~1,351 cm^{-1} and ~2,937 cm^{-1}, respectively, are activated due to the creation of defects and disorders at the surface caused by the chemical or thermal reduction to obtain rGO or graphene. These peaks are the result of intervalley (connects inequivalent points K and K′ in first BZ) and intra-valley (connects two points in the same circle around K or K′) double resonance process, respectively. The D band shows very dispersive behavior to the excitation energy of the laser (Thomsen and Reich, 2000; Ferrari and Basko, 2013). The presence of defects introduces emission of intra-valley and intervalley phonons together resulting in D + D′ peak at ~2,937 cm^{-1}. Therefore, the intensities of these peaks provides a number of qualitative and quantitative information about the nature of the defects (Venezuela et al., 2011). The origin of 2D and 2D′peaks are the processes of momentum conservation by two phonons with opposite wavevectors and hence their activation does not necessarily demand the presence of defects (Ferrari and Basko, 2013).

The graphitization degree of a carbon material is characterized by the I_G/I_D value in the Raman spectra in which I_G = 2837.80 cm^{-1} is the intensity of G band and I_D = 3110.25 cm^{-1} is the intensity of the D band, in this case the relationship I_G/I_D = 1.2 that corresponds to low defect density (Campos et al., 2018;

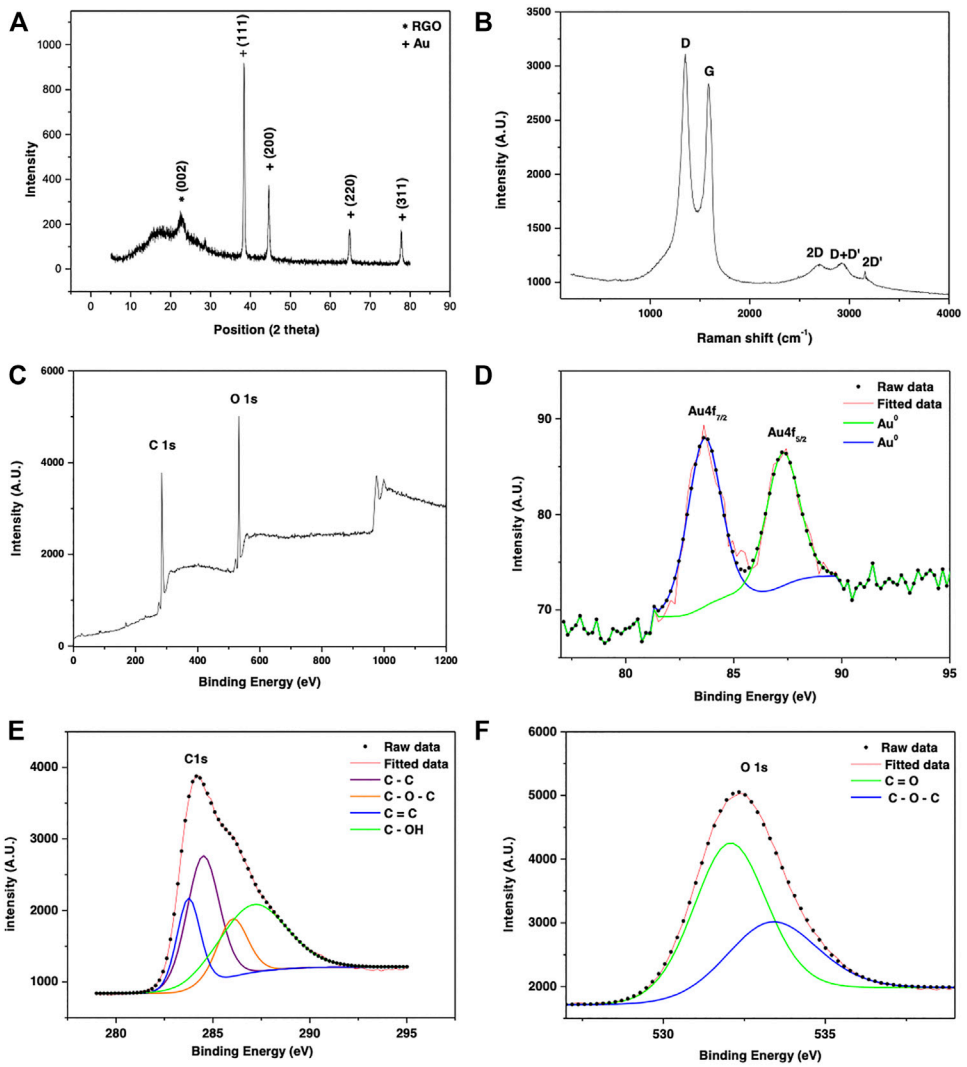

FIGURE 2 | (A) XRD pattern **(B)** Raman and **(C–F)** XPS spectra of the as synthesized graphene-Au composites.

Wu et al., 2018) and could be associated with a chemical interaction or bond between gold nanoparticles and graphene (Movahed et al., 2014), surface dislocation, corrugation, or vacancies (Shin et al., 2010). Additionally, the presence of the 2D peak and D + D' peak indicated improved graphitization and the presence of few layered graphene sheets in the rGO/AuNPs nanocomposite (Otari et al., 2017). Produced because the reduction of GO and the formation of nanoparticles was done *in vitro*, which shows that it is possible to decorate layers of graphene with gold nanoparticles, with a fast and environmentally friendly method of preparation, containing a low density of disorder. **Figure 2C** shows the XPS survey spectra of the rGO/AuNPs nanocomposite, which shows characteristic peaks for C1s and O1s. A detailed analysis of the spectrum also reveals the presence of Au elements. The XPS spectrum at a lower wavenumber region (**Figure 2D**) shows two main peaks of 83.61 and 87.24 eV, equivalent to the binding energies of Au $4f_{7/2}$ and Au $4f_{5/2}$, respectively correspond to the species Au^0 (Otari et al., 2017; Luo et al., 2014) corroborating the presence of gold nanoparticles. Peak associated with C 1s (**Figure 2E**) can be deconvoluted into four consolidated peaks at 283.75, 284.54, 286.05, and 287.02 eV, which can be assigned to the C element in C = C, C - C, C - O – C, and O - OH group, respectively, as shown in the **Figure 2E**. Also, in **Figure 2F**, the peak associated with O 1s is deconvoluted into three peaks at 532, 01 and 533, 15 eV, assigned to the group C = O and C – O – C, respectively. These can be associated with defects on the graphitic structure occurred by the oxidation and reduction reactions during the synthesis process (Gupta et al., 2017).

Microstructural Characterizations of the rGO-Au Composite

The morphology and microstructures of rGO-Au nanocomposites was analyzed by SEM. **Figure 3** shows the low and high magnified SEM images of the as synthesized

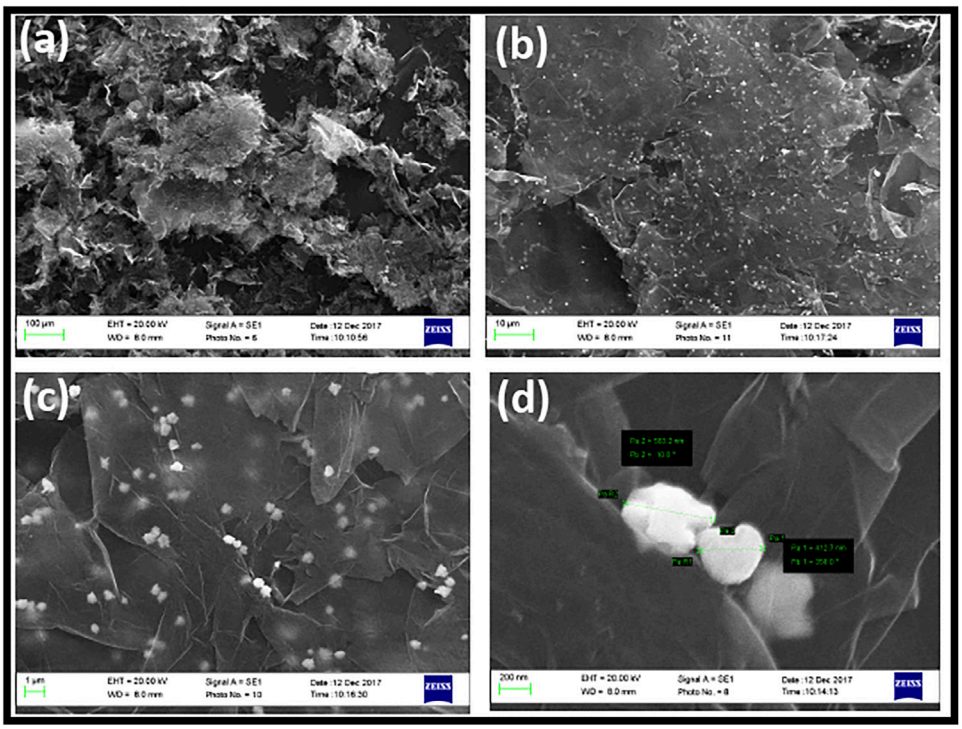

FIGURE 3 | (A–D) Low and high magnification SEM images of the as synthesized graphene-Au composite.

rGO-Au nanocomposites. The low magnification SEM images of the nanocomposite show the various graphene layers composites randomly oriented with a lateral dimension of ~200 μm or less than that (**Figure 3A**). The magnified image in **Figure 3B** shows the large number of homogeneously distributed gold nanoparticles at the surface of rGO. **Figure 3C** shows a narrow size distribution of the synthesized Au nanoparticles on the rGO surface. High magnified image of the Au nanoparticles as shown in **Figure 3D** reveals the size of the particles in the range of 400–500 nm. The chemical composition of the rGO/AuNPs nanocomposite was determined by using energy dispersive X-ray spectroscopy (EDX) analysis. The spectra were recorded at 4 distinct places to confirm the homogeneity of the structure. The EDX analysis in **Figure 4A** clearly shows the presence of mainly carbon and gold content in 53.6, 52.3, 48.7, 59.3 and 24.8, 26.9, 34.9, and 10.7% respectively, corresponding to the region 1, 2, 3, and 4. It clearly reveals the composite mainly consists of carbon with homogeneously distributed gold particles at the surface. The low content of the Au element in the spectra at region 4 can be understood with the elemental mapping at the region where the gold particle is missing which can be clearly observed in **Figure 4A**. A significant amount of oxygen is probably due to the presence of unreduced oxygen functional groups located at the edge ad surface of the graphene sheet. Additionally, the absence of other elements by EDX analysis corroborates the efficiency of the preparation method to obtain rGO/AuNPs. **Figures 4B–F** represent the elemental mapping of the structure which map the different elements at the surface of the synthesized composite.

Electrochemical Measurement in Three Electrode Configurations

The capacitive performance of rGO/AuNPs on Ni foam electrode was evaluated by cyclic voltammograms (CV), galvanostatic charge/discharge (GCD), and electrochemical impedance spectroscopy (EIS). The electrochemical performances of as synthesized electrode material were investigated using three electrode configurations in an electrolyte of 6M KOH which was recently utilized in various reports and is cost effective, too (Zhou et al., 2018; Ma et al., 2019a).

Figure 5A shows the CV of rGO/AuNPs electrode in 6 M KOH solution, in the potential window of -1 – 0 V at the sweep rates of 5 mVs^{-1}, 25 mVs^{-1}, 50 mVs^{-1}, 100 mVs^{-1}, 150 mVs^{-1}, and 200 mVs^{-1}. As shown in the figure, there is a redox peak at the potentials between -0.3 and -0.2 V, which is a typical peak of Ni-foam as shown in the inset of **Figure 5A**. This peak was confirmed by the CV measurement of bare Ni foam in the corresponding potential range. The contribution of the Ni-foam redox peak is minimal compared to CV of the rGO/AuNPs. The shapes of the CV curves clearly confirm the electrostatically double layer capacitive behavior (Arenas Esteban et al., 2020).

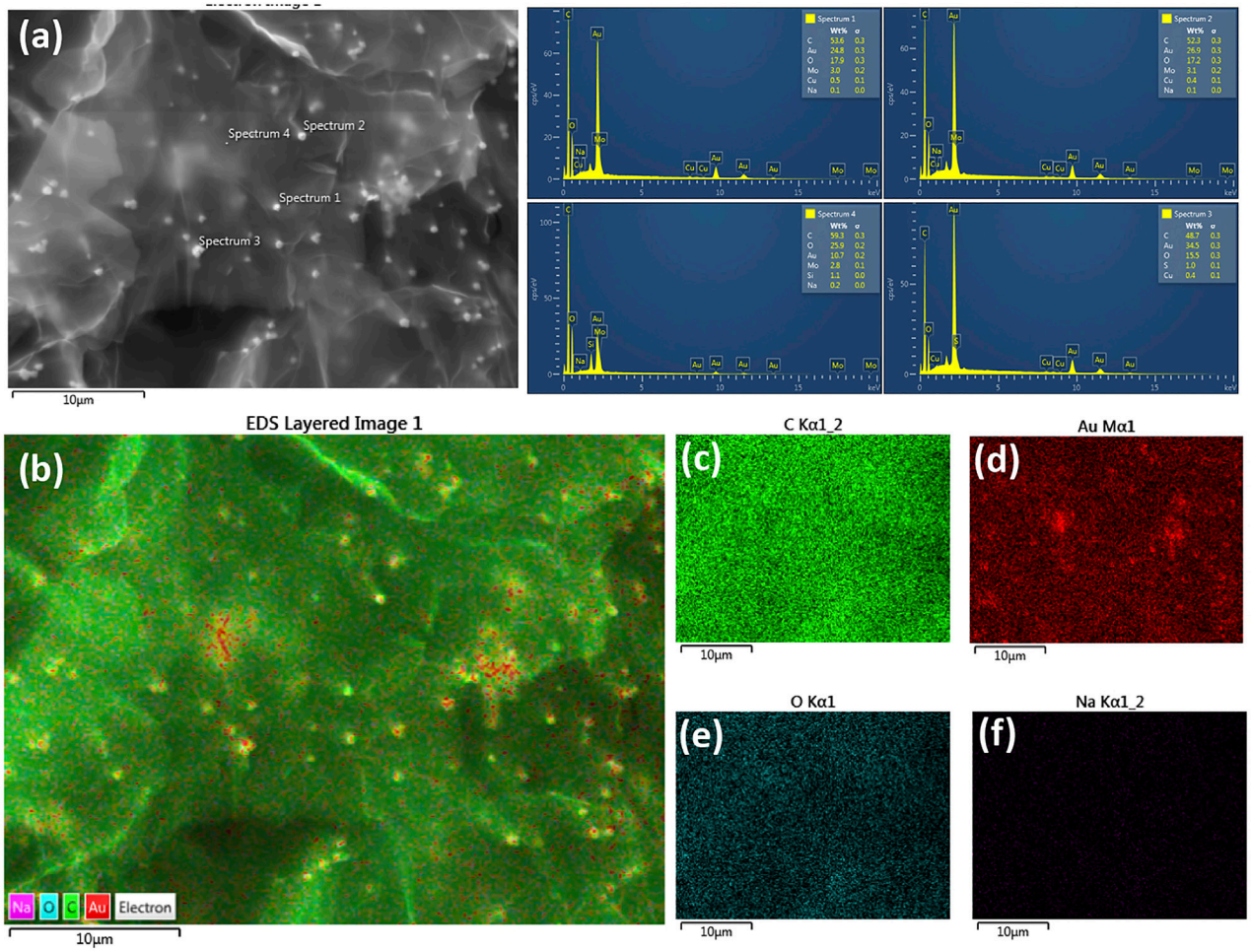

FIGURE 4 | (A) EDXA spectra and **(B–F)** elemental mapping of the rGO- Au nanocomposite.

It can be seen apparently that the current intensity increases with the scan rates, indicating its good electrochemical reversibility (Wang et al., 2009). Specific capacitance of electrodes is calculated from CV curves according to the following equation:

$$C_s = \frac{\int IdV}{mv\Delta V} \quad (1)$$

where I, V, m, and v are the response current density (A), potential (V), mass of active materials (g), and v is the potential scan rate (mVs^{-1}), respectively (Zhang and Pan, 2015).

Figure 5B shows the calculated specific capacitance of rGO-Au nanocomposite electrode as a function of the scan rate. rGO-Au nanocomposite electrode shows maximum and minimum specific capacitances of 303 and 44 Fg^{-1} at the scan rate of 5 and 200 mVs^{-1}, respectively. Whereas specific capacitances of the bare Ni-foam electrode decrease from 32 to 8 F/g at the same scan rate of 5 and 200 mVs^{-1}, respectively, demonstrating that Ni-foam does not contribute much to the specific capacitance of the rGO-Au nanocomposite electrode. As observed, the capacitance of both electrodes decay over the entire range of scan rate because in fast sweep rates only surface porosity is utilized as the ions do not get enough time to get inside the pores and to utilize the overall electrode materials. The deeper sites remain accessible for doing/undoing process. In contrast during slow scan rates ions get time, sufficient to utilize deeper sites also of the electrode materials for doing/undoing process that were not accessible in the case of fast scan rates (Shabani Shayeh et al., 2015b).

The value of the specific capacitance for the rGO-Au composite is comparable to the results obtained by the electrodes made up of reduced graphite oxide and gold nanoparticles. Author Yu et al. reported a specific capacitance value of 257 Fg^{-1} at a scan rate of 2 mVs^{-1}, by the electrodes prepared by electrodeposition on the ITO substrate (Stoller et al., 2008). Shayeh et al. showed high specific capacitance values of 340 Fg^{-1} at a scan rate of 2 mVs^{-1} by using a conductive polymer (PANI) for electrode preparation (Shabani Shayeh et al., 2015a). In our case the high capacitance values are achieved by a very facile method for the

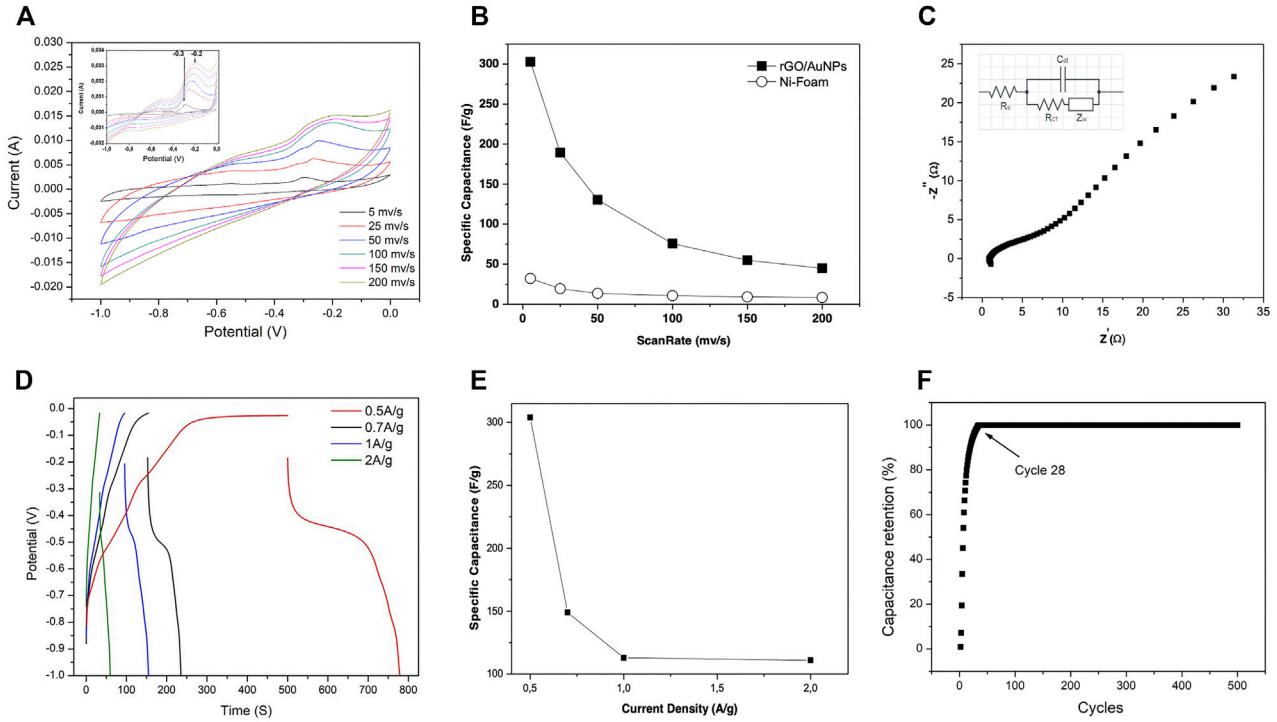

FIGURE 5 | Electrochemical measurement of the graphene-Au composite in three electrode configurations. **(A)** CV curve. **(B)** Specific capacitance of pure Ni foam and rGO-Au composite at different scan rates. **(C)** Nyquist plot. **(D)** Charge discharge curve at different currents densities. **(E)** Specific capacitances at different currents densities. **(F)** Capacity retention of the supercapacitor.

synthesis of electrodes and without using costly conductive polymers. Moreover the use of a greener method for the synthesis of active material is highly appreciated.

For further investigation electrochemical impedance spectroscopy (EIS) was performed on rGO/AuNPs EDLC electrode to generate a Nyquist plot which represents the plot of an imaginary part, in terms of real parts of the complex impedance of the fabricated electrode or device. The spectra were measured in the frequency range of 0.1 – 105 Hz with a time harmonic oscillating electric potential of small amplitude of 0.3 V, as shown in **Figure 5C**. The equivalent circuit model fitting method was utilized to analyze EIS spectra and the inset of **Figure 5C** represents the equivalent RC circuit. The R_s, C_{dl}, R_{ct}, and Z_w values are calculated.

The total internal resistance can be interpreted as the addition of (1) bulk electrolyte resistance (R_s) and (2) charge transfer resistance (R_{ct}). The bulk electrolyte resistance or equivalent series resistance can be attributed to the intrinsic resistance of the active electrode material, resistance of ionic electrolyte and the contact resistance of electrode and current collector. The R_{ct} (represented by the diameter of the semicircle in the plot) is assigned to the electrolyte resistance caused by the faradic reactions in the porous structure. Furthermore, in the plot the nonvertical line represents the ion transport limitations in bulk electrolyte, porous electrode, and non-uniform ion transport at the interface of electrolyte and rough/porous electrode surface (Z_W). Finally, the vertical line results due to electrical double capacitor formation at electrode electrolyte interface (C_{dl}) (Gamby et al., 2001; Mohammad, 2019).

The internal resistance (Rs) of the rGO/AuNPs electrode is 1.45 Ω, manifesting a good conductivity of the electrolyte and the very low internal resistance of the electrode. The charge transfer resistance (R_{ct}) is 2.736 Ω, and demonstrates the excellent electrochemical characteristic of the rGO/AuNPs on Ni foam for the electrode. **Figure 5D** represents the charge–discharge curves of rGO/AuNPs electrode at various specific currents of 0.5, 0.7, 1, and 2 Ag^{-1}. As illustrated in **Figure 5D**, increasing the current density the specific capacitance values decrease due to intercalation of ions at the surface of the active materials in the electrode/electrolyte interface.

On the other hand, while low specific current is used, the specific capacitance increases because there is enough time for insertion and disinsertion of the ions at the surface and at deeper porosities of the active materials in the electrode/electrolyte interface. Here, specific capacitance has been measured according to the charge/discharge curves, using the following equation.

$$C_s = \frac{I}{\left(-\frac{\Delta E}{\Delta t}\right)m} \quad (2)$$

where I is the applied current, -ΔE/Dt is the slope of the discharge curve after the voltage drop at the beginning of each discharge (ESR) and m is the mass of the composite electrodes.

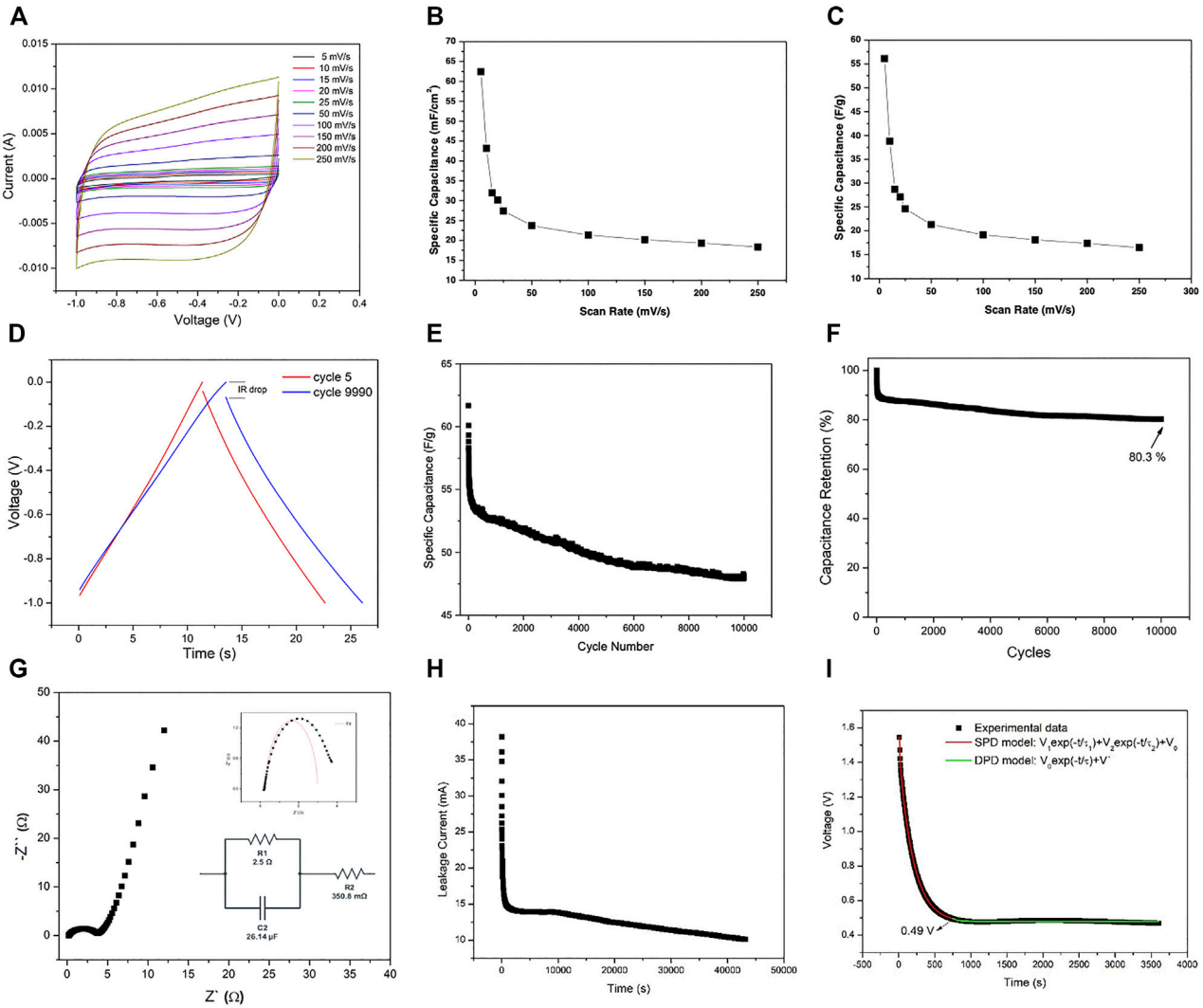

FIGURE 6 | Coin cell performance measurement of the rGO-Au based device. **(A)** CV curve. **(B)** Areal specific capacitance at different scan rates. **(C)** Mass specific capacitance at **(D)** charge discharge curve, **(E)** cyclic stability, **(F)** capacity Retention, and **(G)** Nyquist plot of the supercapacitor device, **(H)** leakage current, and **(I)** self-discharge curves of the device.

For comparison, specific capacitance of the bare activated carbon electrode was also investigated. The obtained CV curve resulted maximum mass and areal specific capacitances of ~27.5 Fg^{-1} and ~31 $mFcm^{-2}$, respectively, at the lowest scan rate of 5 mVs^{-1} (**Supplementary Material**). Which is much less in comparison to the proposed electrode material of rGO-Au. The internal resistance and hence the conductivity of electrode material measured by EIS spectra also shows very high electrode resistance and low conductivity as compared to the rGO-Au electrode material which clearly indicates the enhanced conductivity by the introduction of metallic Au nanomaterials. Calculated internal resistance (R1), charge transfer resistance (R2), and capacitor value (C2) are 849.2 mΩ, 200.9 mΩ, and 12.3 μF, respectively, indicating high resistance and low conductivity of bare AC electrode material for supercapacitor device.

Figure 5E shows the specific capacitance vs. current density curve obtained from the charge and discharge curve of **Figure 5D** and used **Equation (2)**. It is observed that at a current density of 0.5 Ag^{-1}, the specific capacitance is 304 Fg^{-1}, being greater than that reported by other authors for electrodes made with rGO or compounds with rGO. As in the case of multilayer rGO the reported specific capacitance was 247.3 Fg^{-1} at a current density of 0.176 Ag^{-1} whereas the rGO/carbon black exhibited 79 Fg^{-1} at a current density of 1 Ag^{-1} (Anjana et al., 2019) which indicate that the nanoparticles favor the total electronic conductivity of the electrode manufactured as obtained with rGO and the nanoparticles of Au (Zhao and Liu, 2019). Similar values were obtained for Au electrodes, reported by Zhinao Yu et al. (2016), which gave specific capacitance of 288 Fg^{-1} in electrodes RGO-AuNPs. The synthesis of electrode material was carried out by using electrochemical reduction of graphene oxide (GO) at an

indium tin oxide (ITO) electrode followed by an electrodeposition process of loading AuNPs on its surface.

The longevity of the electrode material was examined by using constant current charge-discharge method. **Figure 5F** displays the percentage capacitance retention of rGo-AuNPs with respect to the number of cycles. It was observed that initially for the first 28 cycles the capacity retention increases and then gets saturated up to 500 cycles tasted which shows the longevity of the material while maintaining maximum capacity. The initial increase in the capacitance may be due to activation of the electrode material and more complete interaction with the electrolyte.

Coin Cell Device Measurement

The supercapacitor devices in the form of a coin cell are fabricated in the same way as in industry as shown in **Figure 1B**. The detailed procedure for the fabrication is shown in the Experimental Section. The two-electrode configuration form an asymmetric supercapacitor. The capacitive performance of the device made with rGO-Au nanocomposite electrode is evaluated by cyclic voltammograms (CV), galvanostatic charge/discharge (GCD), and electrochemical impedance spectroscopy (EIS). **Figure 6A** shows the CV of rGO/AuNPs electrode in 6 M KOH solution, in the voltage range of -1 – 0 V at the sweep rates of 5 mVs^{-1}, 10 mVs^{-1}, 15 mVs^{-1}, 20 mVs^{-1}, 25 mVs^{-1}, 50 mVs^{-1}, 100 mVs^{-1}, 150 mVs^{-1}, 200 mVs^{-1}, and 250 mVs^{-1}. As shown in **Figure 6A** the symmetrical and almost rectangular shape of the CV curves indicate an ideal capacitive behavior, good rate capability, and small polarization of the electrode. Akin to the three-electrode configuration, we again observe that the current intensity increases with the scan rates, implying its good electrochemical reversibility.

Figures 6B,C represent the corresponding specific capacities calculated from the CV curves, which were calculated by using the following equation:

$$C_s = \frac{\int IdV}{2\nu\Delta V\Phi} \tag{3}$$

where Φ can be the mass or surface area of the electrode material. **Figure 6B** shows the change of the areal capacitance (Fcm^{-2}) using Φ as the area occupied by the electrode.

The areal specific capacitance values of the device are calculated to be about 62.43 Fcm^{-2} for the lowest scan rate of 5 mVs^{-1} and 18.36 Fcm^{-2} for the highest scan rate value of 250 mVs^{-1}. **Figure 6C** shows the gravimetric capacitance (Fg^{-1}) using Φ as the mass of the electrode. In this case the specific capacitance of 56.09 Fg^{-1} and 16.50 Fg^{-1} were achieved for the lowest and highest scan rate of 5 mVs^{-1} and 250 mVs^{-1}, respectively. The gradual decrease of the specific capacitance when increasing the scan rate is considered as a typical behavior of the electrochemical systems due to the limit of penetration of the electrolytic ions.

Long cycling life is also an important factor to evaluate the device performance for commercial applications. **Figure 6D** shows typical charge-discharge curves of rGO-Au coin cell device calculated at a constant current density of 1 Ag^{-1}. In this case, only the curves corresponding to cycle 5 and 9900 are shown, so that the curves of the first and final cycles can be observed in detail. A triangular shape in each charge and discharge cycle is observed that indicates a good columbic efficiency and ideal capacitive behavior of this device for application as a supercapacitor device. Furthermore, a slight increase can also be observed as the voltage drop (IR) of 0.042 V for the 5th cycle, increases up to 0.069 V for the 9990th cycle, which is related to the internal resistance and appears in the curves during the change of the current sign and vice versa.

Figure 6E shows long-term cyclic stability of the rGO-Au based device tested by continuous charge-discharge measurements at current density of 1 Ag^{-1} for 10,000 cycles. The specific discharge capacitance of the device drops from 61.66 Fg^{-1}, in the first cycle, to 48.00 Fg^{-1}, in the last cycle. Which indicates that the device shows a retention of 80.3% of the initial specific capacitance, as shown in **Figure 6F**. For further confirmation of enhanced electrochemical performance of the composite electrode material, EIS is carried out within the frequency range of 0.1 Hz–1 MHz. The Nyquist plot for the device as depicted in **Figure 6G** suggests that the device behaves like resistors at high frequencies, whereas it acts as a pure capacitor at lower frequencies. In the range of a Nyquist plot of the device, it behaves like a pure condenser and the curve is fitted according to the Levenberg-Merquardt method or DLS according to Gamry instruments' analysis software.[1] The calculated R1, R2, and C2 are 2.5 Ω, 350.8 mΩ, and 26.14 μF, respectively, indicating low and optimum values of these parameters for a supercapacitor device as shown in the red curve of the inset in **Figure 6G** which corresponds to the fitting mentioned above.

Different results of supercapacitor devices based on gold nanoparticles have been shown in the recent literature. Among all the latest reports and the specific capacitance values that are adequate to commercial needs, most of them are poorer or comparable to those reported by us in this work. However, the facile, fast one step, and green approach of synthesis of electrode material proves its supremacy to other reports thus far. The author P. M. Anjara et al. (2019) reports specific capacitance values of 80 Fg^{-1} to 1 Ag^{-1} and 93% capacity retention after 5000 charge/discharge cycles with a device based on AuNPs/porous carbon electrodes. Yang Chen et al. (2019) manufactured an ultrathin Au/graphene device that shows a specific capacitance of 81 μFcm^{-2} at 0.1 Vs^{-1} and a retention of 87.5% after 1,800 cycles and Li et al. (2016) proposed a device made with rGO/AuNPs micro electrodes with a specific capacitance of 0.77 mFcm^{-2} and a retention ranging from 99% to 50 mVs^{-1} up to 80.3% to 1 mVs^{-1} after 10,000 cycles. In comparison to the abovementioned reports, the proposed device by us exhibits superior values benefitted over with the synthesis of electrode materials by a simple, one step, cost-effective, and ecofriendly way.

[1]https://www.gamry.com/application-notes/EIS/user-defined-components-for-eis-modeling/, (n.d.).

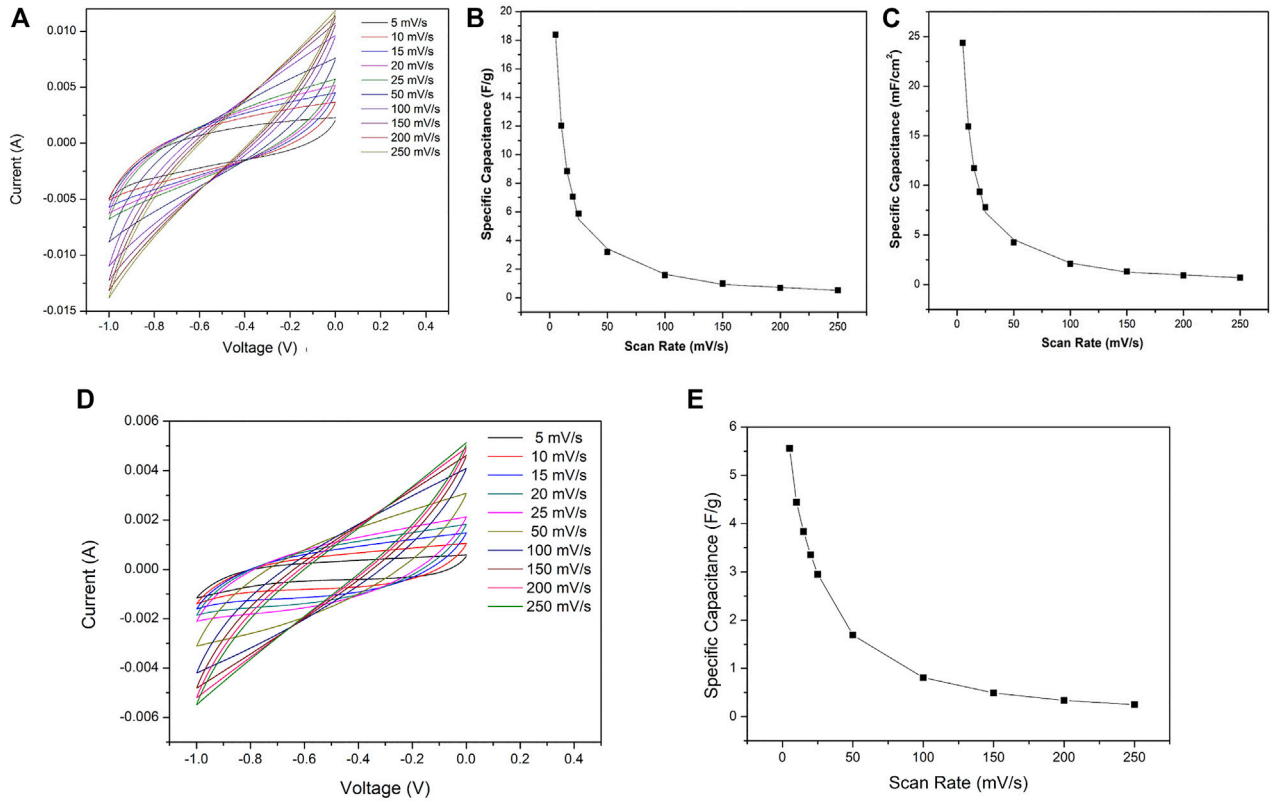

FIGURE 7 | (A) CV curve of the coin cell device fabricated with as synthesized rGO electrode in two electrode configurations obtained by the reduction with ascorbic acid. **(B)** Calculated mass specific capacitance at different scan rates. **(C)** Calculated areal specific capacitance at different scan rates. **(D)** CV curve of a coin cell device fabricated by electrode material of bare activated carbon and **(E)** calculated mass specific capacitance at different scan rates.

To get better insight into the proposed coin cell device, leakage current and self-discharge measurements were done. The leakage current was carried out at 2 V for 12 h and the self-discharge was done for 2 h at 2 V and the self-discharge was observed for 20 min. **Figure 6H** and **Figure 6I** show the leakage current and self-discharge curves of the proposed device. Leakage current drops drastically within 20 min and decays from 14 to 10 mA, up to 14.5 h. As a result of the leakage current, the open-circuit voltage of the supercapacitor is rapidly decreased within the first 10 min and gently subsequently. In the self-discharge study, the curve was fitted according to two models as proposed in the literature (Zhang et al., 2011a). During the first few minutes the predominant model is the divided potential driving (DPD) as shown in red in the graph. The rapid decrease in voltage is due to the interaction of the electrolyte ions with the front layers of the electrode material that induces a high energy loss (Zhang et al., 2011b; Chen et al., 2014; Haque et al., 2021). After the first 10 min the predominant model is the single potential driving (SPD) which is shown in green which is the common one to describe the self-discharge in supercapacitors. In model SPD ($V = V_0 \exp(-t/\tau) + V'$) the τ is a characteristic parameter specifying the self-discharge rate and determined by the mobility of ions and the magnitude of the potential field. Higher τ refers to the lower self-discharge rate for the device (τ = 1,343 s). In the DPD model, the larger time constant τ_1 = 1017 s represents the potential-driving self-discharge part associated with a group of electrolyte ions with a slower self-discharge rate, and the smaller τ_2 = 69 s represents the group of ions with a faster self-discharge rate. The transition between these models is ascribed to the intrinsic bonding variation between the electrolyte ions and the electrodes in the charged state due to the interaction between the functional groups present at the electrode material's surface/edges (rGO: hydroxyl, carboxyl, epoxy groups due to the reduction of GO) and the electrolyte ions (Ricketts and Ton-That, 2000; Mishra et al., 2019).

For comparison, CV measurement of the coin cell device in two electrode configurations fabricated with as synthesized rGO electrode was also examined as shown in **Figure 7**. The curve (**Figure 7A**) represents a typical electrostatically double layer capacitance behavior. The calculated maximum specific mass capacitance and areal capacitance are ~18 Fg^{-1} and ~25 $mFcm^{-2}$, respectively, at a scan rate of 5 mVs^{-1} (**Figures 7B,C**). These are comparatively very low to the coin cell device fabricated by the rGO-Au electrode material. The conductivity of the material from which the electrodes of a supercapacitor are made affects the capacitance

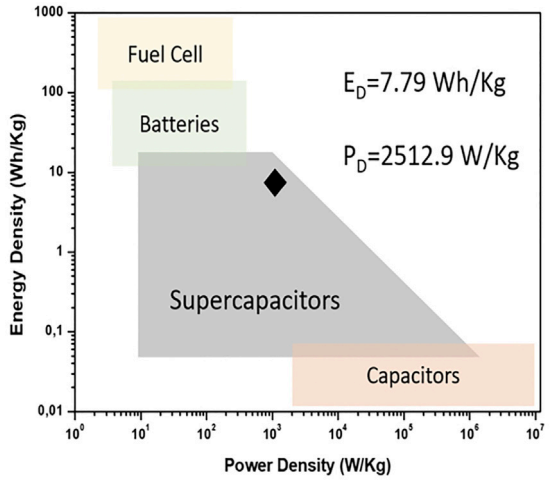

FIGURE 8 | Ragone Plot for the proposed supercapacitor device based on rGO/AuNPs.

of the device referring to a material with high conductivity that improves the capacitance. Graphene is used in supercapacitors because of its large surface area but has a drawback, that when electrodes are prepared for the device, the graphene layers collapse allowing contact among them and hence an increase in the internal resistance. The most effective way to avoid it is to place or anchor nanoparticles between the layers to avoid contact between them and simultaneously maintaining good conductivity of graphene. If these particles have a high value of conductivity, this value is added in the system which improves the overall capacitance. The capacitance performance of the device is only with electrostatic process. The Au nanoparticles are very stable and have no faradaic effect, which makes them ideal to be used in combination with other materials for the electrode preparation for supercapacitors (Ma et al., 2019b). In addition to high conductivity, *in situ* decoration of Au nanoparticles on the surface and interlayers of rGO restricts the collapsing of a graphene structure and henceforth helps to maintain the high surface area of synthesized electrode material. That is why the device based on the electrodes with rGO-Au nanoparticles exhibited much better performance than bare rGO.

Activated carbon (AC) is one of the earliest and extensively exploited materials for electrode preparation of commercial supercapacitors due to its high specific surface area, electrochemical stability, abundance, low cost, and environmental friendliness (Simon and Gogotsi, 2008; Lv et al., 2012; Shang et al., 2016). In some of the commercial supercapacitors, the reported specific capacitance lies between 100 and 200 Fg^{-1} in three electrode configurations.

One way to reduce the cost of supercapacitor devices is to manufacture the electrodes with a portion of activated carbon, which guarantees the electrical conduction and the good electrochemical performance of the device. In addition, for the electrode fabrication, it is necessary to make a paste with active material and binder. If these two materials are mixed with the activated carbon the paste has a better physical stability that makes the fabrication of the electrodes easier and helps in the long-term electrochemical measurements of the devices. The CV curve at different scan rates and calculated specific capacitance of a coin cell device fabricated by utilizing bare activated carbon as an electrode material are shown in **Figure 7D** and **Figure 7E**. The calculated highest specific capacitance in this case is 5.5 Fg^{-1} at the scan rate of 5 mVs^{-1}, which is approximately 10% of the specific capacitance of the proposed device with rGO-Au active material.

Figure 8 shows the Ragone plot of the as-assembled device. This diagram shows the energy and power density of the device fabricated with rGO-Au nanocomposite. To calculate the energy density, the following equation is used:

$$E_D = \frac{1}{2} C_s (\Delta V)^2 \tag{4}$$

where C_s is the specific capacitance, taken from the CV curves (**Figure 6B**) at 5 mVs^{-1} and ΔV is the voltage window. Also, to calculate the power density the following equation is used:

$$P_D = \frac{E_D}{\Delta t}, \tag{5}$$

where Δt is the rate of discharge of the cell. The Ragone plot of the device manufactured with rGO-Au shows an energy density of 7.79 WH kg^{-1} and a power density of 2512.9 W Kg^{-1}, which are within the parameters accepted and anticipated for a commercially suitable supercapacitor device. **Figure 8** shows schematically the ranges of energy densities and power density in which different devices work and the range where our device corresponds for, predicting that the parameters corresponding to the supercapacitor of this study are within the optimal range of operation. The excellent values of energy density and power density that we report in this work are comparable with the device fabricated with a complex methodology in 3D reduced graphite oxide (3DrGO) with a conductive polymer, deposited on a polypyrrol (PPy) network on a pristine gold (NPAu) nanoporous chip with which a solid state, flexible, and symmetrical super capacitor (PPy-3DrGO/NPAu) was manufactured as reported by Taniya Purkait et al. (Zhang et al., 2011a; Purkait et al., 2018) which shows an energy density value of 98.48 mWh and power density of 19.68 W.

CONCLUSION

A highly efficient, low cost, easy to manufacture, commercially viable, and above all eco-friendly green supercapacitor is designed. The proposed coin cell supercapacitor device exhibits maximum areal and mass specific capacitance of 62.43 $mFcm^{-2}$ and 56.09 Fg^{-1}, respectively, that is very high among all reported graphene based composite devices and retains capacity up to 80% even after 10,000 cycles. This green method of synthesis for active materials can further be utilized for various other graphene-based metal composites (such as Ag and

Cu) and supercapacitor devices can be fabricated for widespread commercialization.

EXPERIMENTAL SECTIONS

Synthesis of GO

All the chemicals used in the experiment were of analytical grade and bought from Sigma Aldrich. Graphene oxide (GO) was synthesized from graphite powder using Hummer's method. In brief, 1 g of graphite and 100 ml of sulfuric acid were mixed followed by the addition of 6 g of potassium permanganate ($KMnO_4$) under constant stirring. Mixing was done in a beaker kept at 5°C in an ice bath and then the mixture was stirred at room temperature for 2 h. The resulting solution was sonicated for 1 h and then stirred for 48 h. This solution was diluted by adding 400 ml of water under vigorous stirring for 1 h, which resulted in the final product of GO.

Synthesis of rGO/AuNPs Composites

The rGO-AuNPs composite was synthesized by chemical reduction process by using gold (III) chloride ($AuCl_3$) as a precursor salt. Initially the 50.6 mg de $AuCl_3$ was dissolved into 100 ml of distilled water under constant magnetic stirring for 10 min. Then after 20 ml of graphene oxide as obtained in the previous section was added to the solution under magnetic stirring for 10 min at T = 125°C. Finally, 5 g of ascorbic acid ($C_6H_8O_6$) and 0.4 g (0.1M) of NaOH powder was added to the solution and continuous stirring for 30 min and the temperature was maintained at 125°C. The temperature and pH of the solution were measured before and after the addition of NaOH and $C_6H_8O_6$ in the solution. The final hydrophobic product got settled down rapidly which was cleaned with distilled water several times to remove any byproducts and dried by freeze drying process for further characterizations and electrode preparation for the supercapacitor's electrodes and device.

Structural/Microstructural/Spectral Characterizations

The crystallographic structure of the as-prepared materials was confirmed by powder X-ray diffraction (XRD) by XRD-Shimadzu6000 powder diffractometer (Cu-Ka radiation, 40 kV and 30 mA). The microstructural characterization and elemental analysis were done by scanning electron microscope (SEM Zeiss at 30 kV) whereas Raman spectrometer was utilized for spectral characterizations. The elements present rGO/AuNPs as well as their chemical state were identified by XPS analysis by utilizing x-ray photoelectron microscopy by using a Surface Analysis Station 1 (model: XPS RQ300/2) and a monochrome Al source (1486.6 eV).

Standard Three-Electrode Cell Assembly

The electrode was prepared by mixing all together; a binder poly (methymethacrylate) (PMMA), commercial grade activated carbon, and synthesized active material rGO/AuNPs in a solvent acetone in proportions of 10, 30, and 60%, respectively, to obtain a homogeneous paste. The measured mass of the active material was 8.4 mg. This paste was coated on a 1.00 cm^2 area of Ni-foam sheet and kept for 1 h at ambient condition to evaporate the solvent. Finally, the electrode was prepared by connecting a copper wire to the Ni-foam with conducting silver paint.

Coin Cell Supercapacitor Device Fabrication

For the coin cell device fabrication two electrode configurations were utilized. Both the electrodes were prepared as described in three electrode configurations but on stainless steel substrate instead of Ni foam and in this case used 14.7 mg of active materials. The homogeneous solution was spin coated on a circular stainless-steel sheet to obtain a homogeneous thin film by utilizing a spin coating technique and the electrode was dried at ambient condition. The electrodes were separated by a commercially available filter paper soaked in 6M KOH solution and this configuration was sandwiched between a stainless-steel coin cell, cap, and can followed by pressing with hydraulic pressure machine (pressure of 1.33 MPa) to obtain the coin cell device.

Electrochemical Characterization

The electrochemical properties and capacitance measurements of supercapacitor electrodes were studied in a two-electrode and three-electrode system by cyclic voltammetry (CV), electrochemical impedance spectroscopy (EIS), and charge-discharge by using an Interface 5000E Gamry instrument. For the electrochemical measurements in a three-electrode arrangement a bright Pt plate and Ag/AgCl electrode were used as the counter electrode and reference electrode, respectively. The CV response of the electrodes and coin cell were measured at different scan rates varying from 5 mVs^{-1} to 250 mVs^{-1}. Voltammetry testing was carried out at voltages between -1 and 0 V by using 6 M aqueous KOH solution as an electrolyte. Impedance spectroscopy measurements were carried out in the frequency range of 1 MHz to 0.1 Hz.

DATA AVAILABILITY STATEMENT

The original contributions presented in the study are included in the article/**Supplementary Material**, further inquiries can be directed to the corresponding author.

AUTHOR CONTRIBUTIONS

LV: Planned and performed various experiments, data analysis, helped in writing manuscripts. DS Ideas, conceptualization, planning of the experiments, analysis of results and scientific discussions, wrote the manuscript.

FUNDING

This work was funded by ANID – Millennium Science Initiative Program—ICN17_012 through the Millennium Institute for Research in Optics (MIRO) and ANID- Fondecyt Postdoctorado 3210225.

SUPPLEMENTARY MATERIAL

The Supplementary Material for this article can be found online at: https://www.frontiersin.org/articles/10.3389/fenrg.2021.794604/full#supplementary-material

REFERENCES

Abdolhosseinzadeh, S., Asgharzadeh, H., and Seop Kim, H. (2015). Fast and Fully-Scalable Synthesis of Reduced Graphene Oxide. *Sci. Rep.* 5, 1–7. doi:10.1038/srep10160

Anjana, P. M., Bindhu, M. R., and Rakhi, R. B. (2019). Green Synthesized Gold Nanoparticle Dispersed Porous Carbon Composites for Electrochemical Energy Storage. *Mater. Sci. Energ. Tech.* 2, 389–395. doi:10.1016/j.mset.2019.03.006

Aphale, A., Maisuria, K., Mahapatra, M. K., Santiago, A., Singh, P., and Patra, P. (2015). Hybrid Electrodes by *In-Situ* Integration of Graphene and Carbon-Nanotubes in Polypyrrole for Supercapacitors. *Sci. Rep.* 5, 14445. doi:10.1038/srep14445

Arenas Esteban, D., Guerrero Martínez, A., Carretero González, J., Birss, V. I., Otero-Díaz, L. C., and Ávila Brande, D. (2020). Tunable Supercapacitor Materials Derived from Hydrochar/Gold Nanograpes. *ACS Appl. Energ. Mater.* 3, 9348–9359. doi:10.1021/acsaem.0c01711

Azadfalah, M., Sedghi, A., Hosseini, H., and Kashani, H. (2021). Cobalt Based Metal Organic Framework/Graphene Nanocomposite as High Performance Battery-type Electrode Materials for Asymmetric Supercapacitors. *J. Energ. Storage* 33, 101925. doi:10.1016/J.EST.2020.101925

Balandin, A. A., Ghosh, S., Bao, W., Calizo, I., Teweldebrhan, D., Miao, F., et al. (2008). Superior Thermal Conductivity of Single-Layer Graphene. *Nano Lett.* 8, 902–907. doi:10.1021/nl0731872

Campos, J. L. E., Miranda, H., Rabelo, C., Sandoz-Rosado, E., Pandey, S., Riikonen, J., et al. (2018). Applications of Raman Spectroscopy in Graphene-Related Materials and the Development of Parameterized PCA for Large-Scale Data Analysis. *J. Raman Spectrosc.* 49, 54–65. doi:10.1002/jrs.5225

Chen, L., Bai, H., Huang, Z., and Li, L. (2014). Mechanism Investigation and Suppression of Self-Discharge in Active Electrolyte Enhanced Supercapacitors. *Energy Environ. Sci.* 7, 1750–1759. doi:10.1039/c4ee00002a

Chen, Y., Fu, X.-Y., Yue, Y.-Y., Zhang, N., Feng, J., and Sun, H.-B. (2019). Flexible and Transparent Supercapacitor Based on Ultrathin Au/graphene Composite Electrodes. *Appl. Surf. Sci.* 467-468, 467104–468111. doi:10.1016/j.apsusc.2018.10.093

Chen, Y., Li, Y., Sun, D., Tian, D., Zhang, J., and Zhu, J.-J. (2011). Fabrication of Gold Nanoparticles on Bilayer Graphene for Glucose Electrochemical Biosensing. *J. Mater. Chem.* 21, 7604–7611. doi:10.1039/c1jm10293a

Das Jana, I., Kumbhakar, P., Banerjee, S., Gowda, C. C., Kedia, N., Kuila, S. K., et al. (2021). Copper Nanoparticle-Graphene Composite-Based Transparent Surface Coating with Antiviral Activity against Influenza Virus. *ACS Appl. Nano Mater.* 4, 352–362. doi:10.1021/acsanm.0c02713

Du, Q., Zheng, M., Zhang, L., Wang, Y., Chen, J., Xue, L., et al. (2010). Preparation of Functionalized Graphene Sheets by a Low-Temperature thermal Exfoliation Approach and Their Electrochemical Supercapacitive Behaviors. *Electrochimica Acta* 55, 3897–3903. doi:10.1016/j.electacta.2010.01.089

Emiru, T. F., and Ayele, D. W. (2017). Controlled Synthesis, Characterization and Reduction of Graphene Oxide: A Convenient Method for Large Scale Production. *Egypt. J. Basic Appl. Sci.* 4, 74–79. doi:10.1016/J.EJBAS.2016.11.002

Ferrari, A. C., and Basko, D. M. (2013). Raman Spectroscopy as a Versatile Tool for Studying the Properties of Graphene. *Nat. Nanotech.* 8, 235–246. doi:10.1038/nnano.2013.46

Ferrari, A. C., Meyer, J. C., Scardaci, V., Casiraghi, C., Lazzeri, M., Mauri, F., et al. (2006). Raman Spectrum of Graphene and Graphene Layers. *Phys. Rev. Lett.* 97, 187401. doi:10.1103/PhysRevLett.97.187401

Gamby, J., Taberna, P. L., Simon, P., Fauvarque, J. F., and Chesneau, M. (2001). Studies and Characterisations of Various Activated Carbons Used for Carbon/carbon Supercapacitors. *J. Power Sourc.* 101, 109–116. doi:10.1016/S0378-7753(01)00707-8

Geim, A. K., and Novoselov, K. S. (2007). The Rise of Graphene. *Nat. Mater.* 6, 183–191. doi:10.1038/nmat1849

Gupta, B., Kumar, N., Panda, K., Kanan, V., Joshi, S., and Visoly-Fisher, I. (2017). Role of Oxygen Functional Groups in Reduced Graphene Oxide for Lubrication. *Sci. Rep.* 7, 45030. doi:10.1038/srep45030

Haque, M., Li, Q., Rigato, C., Rajaras, A., Smith, A. D., Lundgren, P., et al. (2021). Identification of Self-Discharge Mechanisms of Ionic Liquid Electrolyte Based Supercapacitor under High-Temperature Operation. *J. Power Sourc.* 485, 229328. doi:10.1016/j.jpowsour.2020.229328

Hosseini, H., and Shahrokhian, S. (2018). Advanced Binder-free Electrode Based on Core-Shell Nanostructures of Mesoporous Co3V2O8-Ni3V2O8 Thin Layers@porous Carbon Nanofibers for High-Performance and Flexible All-Solid-State Supercapacitors. *Chem. Eng. J.* 341, 10–26. doi:10.1016/J.CEJ.2018.02.019

Hosseini, H., and Shahrokhian, S. (2019). Self-supported Nanoporous Zn-Ni-Co/Cu Selenides Microball Arrays for Hybrid Energy Storage and Electrocatalytic Water/urea Splitting. *Chem. Eng. J.* 375, 122090. doi:10.1016/J.CEJ.2019.122090

Hosseini, H., and Shahrokhian, S. (2018). Vanadium Dioxide-Anchored Porous Carbon Nanofibers as a Na+ Intercalation Pseudocapacitance Material for Development of Flexible and Super Light Electrochemical Energy Storage Systems. *Appl. Mater. Today* 10, 72–85. doi:10.1016/J.APMT.2017.11.011

Ioni, Y., Buslaeva, E., and Gubin, S. (2016). Synthesis of Graphene with Noble Metals Nanoparticles on its Surface. *Mater. Today Proc.* 3, S209–S213. doi:10.1016/J.MATPR.2016.02.035

Janani, S., Sudha, K. S. R., Ellappan, P., and Miranda, L. R. (2016). Photodegradation of Methylene Blue Using Magnetically Reduced Graphene Oxide Bismuth Oxybromide Composite. *J. Environ. Chem. Eng.* 4, 534–541. doi:10.1016/J.JECE.2015.10.043

Jokar, E., Shahrokhian, S., zad, A. I., Asadian, E., and Hosseini, H. (2018). An Efficient Two-step Approach for Improvement of Graphene Aerogel Characteristics in Preparation of Supercapacitor Electrodes. *J. Energ. Storage* 17, 465–473. doi:10.1016/J.EST.2018.04.014

Ke, Q., and Wang, J. (2016). Graphene-based Materials for Supercapacitor Electrodes - A Review. *J. Materiomics* 2, 37–54. doi:10.1016/j.jmat.2016.01.001

Khan, M., Tahir, M. N., Adil, S. F., Khan, H. U., Siddiqui, M. R. H., Al-Warthan, A. A., et al. (2015). Graphene Based Metal and Metal Oxide Nanocomposites: Synthesis, Properties and Their Applications. *J. Mater. Chem. A.* 3, 18753–18808. doi:10.1039/c5ta02240a

Kötz, R., and Carlen, M. (2000). Principles and Applications of Electrochemical Capacitors. *Electrochimica Acta* 45, 2483–2498. doi:10.1016/s0013-4686(00)00354-6

Li, R.-Z., Peng, R., Kihm, K. D., Bai, S., Bridges, D., Tumuluri, U., et al. (2016). High-rate In-Plane Micro-supercapacitors Scribed onto Photo Paper Using *In Situ* Femtolaser-Reduced Graphene oxide/Au Nanoparticle Microelectrodes. *Energ. Environ. Sci.* 9, 1458–1467. doi:10.1039/c5ee03637b

Luo, J., Zhang, N., Liu, R., and Liu, X. (2014). *In Situ* green Synthesis of Au Nanoparticles onto Polydopamine-Functionalized Graphene for Catalytic Reduction of Nitrophenol. *RSC Adv.* 4, 64816–64824. doi:10.1039/C4RA11950A

Lv, Y., Gan, L., Liu, M., Xiong, W., Xu, Z., Zhu, D., et al. (2012). A Self-Template Synthesis of Hierarchical Porous Carbon Foams Based on Banana Peel for Supercapacitor Electrodes. *J. Power Sourc.* 209, 152–157. doi:10.1016/j.jpowsour.2012.02.089

Ma, H., Chen, Z., Gao, X., Liu, W., and Zhu, H. (2019). 3D Hierarchically Gold-Nanoparticle-Decorated Porous Carbon for High-Performance Supercapacitors. *Sci. Rep.* 9, 1–10. doi:10.1038/s41598-019-53506-6

Ma, H., Chen, Z., Gao, X., Liu, W., and Zhu, H. (2019). 3D Hierarchically Gold-Nanoparticle-Decorated Porous Carbon for High-Performance Supercapacitors. *Sci. Rep.* 9, 17065. doi:10.1038/s41598-019-53506-6

Mishra, R. K., Choi, G. J., Sohn, Y., Lee, S. H., and Gwag, J. S. (2019). Reduced Graphene Oxide Based Supercapacitors: Study of Self-Discharge Mechanisms, Leakage Current and Stability via Voltage Holding Tests. *Mater. Lett.* 253, 250–254. doi:10.1016/j.matlet.2019.06.073

Mohammad, D. L. (2019). *Jawaid, Akil Ahmad, Graphene-Based Nanotechnologies for Energy and Anvironmental*. Amsterdam: Elsevier.

Movahed, S. K., Fakharian, M., Dabiri, M., and Bazgir, A. (2014). Gold Nanoparticle Decorated Reduced Graphene Oxide Sheets with High Catalytic Activity for Ullmann Homocoupling. *RSC Adv.* 4, 5243. doi:10.1039/c3ra45518a

Otari, S. V., Kumar, M., Anwar, M. Z., Thorat, N. D., Patel, S. K. S., Lee, D., et al. (2017). Rapid Synthesis and Decoration of Reduced Graphene Oxide with Gold Nanoparticles by Thermostable Peptides for Memory Device and Photothermal Applications. *Sci. Rep.* 7, 10980. doi:10.1038/s41598-017-10777-1

Purkait, T., Singh, G., Kamboj, N., Das, M., and Dey, R. S. (2018). All-porous Heterostructure of Reduced Graphene Oxide-Polypyrrole-Nanoporous Gold for a Planar Flexible Supercapacitor Showing Outstanding Volumetric Capacitance and Energy Density. *J. Mater. Chem. A.* 6, 22858–22869. doi:10.1039/c8ta07627h

Ramachandran, R., Mani, V., Chen, S.-M., Ramiah, S., and Lou, B. (2013). Recent Trends in Graphene Based Electrode Materials for Energy Storage Devices and Sensors Applications. *Int. J. Electrochem. Sci.* 8, 11680–11694.

Ricketts, B. W., and Ton-That, C. (2000). Self-discharge of Carbon-Based Supercapacitors with Organic Electrolytes. *J. Power Sourc.* 89, 64–69. doi:10.1016/S0378-7753(00)00387-6

Rodríguez-Otamendi, D. I., Meza-Laguna, V., Acosta, D., Álvarez-Zauco, E., Huerta, L., Basiuk, V. A., et al. (2021). Eco-friendly Synthesis of Graphene Oxide-Silver Nanoparticles Hybrids: The Effect of Amine Derivatization. *Diamond Relat. Mater.* 111, 108208. doi:10.1016/j.diamond.2020.108208

Sahoo, G., Sarkar, N., Sahu, D., and Swain, S. K. (2017). Nano Gold Decorated Reduced Graphene Oxide Wrapped Polymethylmethacrylate for Supercapacitor Applications. *RSC Adv.* 7, 2137–2150. doi:10.1039/c6ra26930c

Shabani Shayeh, J., Ehsani, A., Ganjali, M. R., Norouzi, P., and Jaleh, B. (2015). Conductive Polymer/reduced Graphene oxide/Au Nano Particles as Efficient Composite Materials in Electrochemical Supercapacitors. *Appl. Surf. Sci.* 353, 594–599. doi:10.1016/j.apsusc.2015.06.066

Shabani Shayeh, J., Norouzi, P., and Ganjali, M. R. (2015). Studying the Supercapacitive Behavior of a Polyaniline/nano-Structural Manganese Dioxide Composite Using Fast Fourier Transform Continuous Cyclic Voltammetry. *RSC Adv.* 5, 20446–20452. doi:10.1039/C4RA16801A

Shang, T.-X., Zhu, Y.-M., and Jin, X.-J. (2016). Preparation of Disused Composite Panels-Based Activated Carbon by Microwave Induced Activation for High Performance of Electric Double-Layer Capacitors: Microwave Power Effects. *Sci. Adv. Mater.* 8, 1101–1107. doi:10.1166/sam.2016.2707

Shin, Y. J., Wang, Y., Huang, H., Kalon, G., Wee, A. T. S., Shen, Z., et al. (2010). Surface-Energy Engineering of Graphene. *Langmuir* 26, 3798–3802. doi:10.1021/la100231u

Simon, P., and Gogotsi, Y. (2008). Materials for Electrochemical Capacitors. *Nat. Mater* 7, 845–854. doi:10.1038/nmat2297

Stoller, M. D., Park, S., Zhu, Y., An, J., and Ruoff, R. S. (2008). Graphene-Based Ultracapacitors. *Nano Lett.* 8, 3498–3502. doi:10.1021/nl802558y

Sze, P.-W., Lan, W.-H., Chou, D.-W., Liu, N.-H., Feng, S.-W., and Huang, C.-J. (2017). The Effect of Ascorbic Acid Using in Electrochemical Method to Synthesize Gold Nanoparticles. *J. Nanosci. Nanotechnol.* 17, 5735–5739. doi:10.1166/jnn.2017.13825

Tan, Y., Li, Y., Kong, L., Kang, L., and Ran, F. (2018). Synthesis of Ultra-small Gold Nanoparticles Decorated onto NiO Nanobelts and Their High Electrochemical Performance. *Dalton Trans.* 47, 8078–8086. doi:10.1039/c8dt01735b

Thomsen, C., and Reich, S. (2000). Double Resonant Raman Scattering in Graphite. *Phys. Rev. Lett.* 85, 5214–5217. doi:10.1103/PhysRevLett.85.5214

Tommalieh, M. J., Awwad, N. S., Ibrahium, H. A., and Menazea, A. A. (2021). Characterization and Electrical Enhancement of PVP/PVA Matrix Doped by Gold Nanoparticles Prepared by Laser Ablation. *Radiat. Phys. Chem.* 179, 109195. doi:10.1016/j.radphyschem.2020.109195

Venezuela, P., Lazzeri, M., and Mauri, F. (2011). Theory of Double-Resonant Raman Spectra in Graphene: Intensity and Line Shape of Defect-Induced and Two-Phonon Bands. *Phys. Rev. B* 84, 035433. doi:10.1103/PhysRevB.84.035433

Wang, Y., Shi, Z., Huang, Y., Ma, Y., Wang, C., Chen, M., et al. (2009). Supercapacitor Devices Based on Graphene Materials. *J. Phys. Chem. C* 113, 13103–13107. doi:10.1021/jp902214f

Wu, J.-B., Lin, M.-L., Cong, X., Liu, H.-N., and Tan, P.-H. (2018). Raman Spectroscopy of Graphene-Based Materials and its Applications in Related Devices. *Chem. Soc. Rev.* 47, 1822–1873. doi:10.1039/c6cs00915h

Yin, P. T., Kim, T.-H., Choi, J.-W., and Lee, K.-B. (2013). Prospects for Graphene-Nanoparticle-Based Hybrid Sensors. *Phys. Chem. Chem. Phys.* 15, 12785–12799. doi:10.1039/c3cp51901e

Yu, Z., Sun, S., and Huang, M. (2016). Electrodeposition of Gold Nanoparticles on Electrochemically Reduced Graphene Oxide for High Performance Supercapacitor Electrode Materials. *Int. J. Electrochem. Sci.* 11, 3643–3650. doi:10.20964/110448

Zhang, Q., Rong, J., Ma, D., and Wei, B. (2011). The Governing Self-Discharge Processes in Activated Carbon Fabric-Based Supercapacitors with Different Organic Electrolytes. *Energ. Environ. Sci.* 4, 2152–2159. doi:10.1039/c0ee00773k

Zhang, Q., Rong, J., and Wei, B. (2011). A Divided Potential Driving Self-Discharge Process for Single-Walled Carbon Nanotube Based Supercapacitors. *RSC Adv.* 1, 989–994. doi:10.1039/C1RA00318F

Zhang, S., and Pan, N. (2015). Supercapacitors Performance Evaluation. *Adv. Energ. Mater.* 5, 1401401. doi:10.1002/aenm.201401401

Zhang, Y., Tang, T.-T., Girit, C., Hao, Z., Martin, M. C., Zettl, A., et al. (2009). Direct Observation of a Widely Tunable Bandgap in Bilayer Graphene. *Nature* 459, 820–823. doi:10.1038/nature08105

Zhao, G., and Liu, G. (2019). Electrochemical Deposition of Gold Nanoparticles on Reduced Graphene Oxide by Fast Scan Cyclic Voltammetry for the Sensitive Determination of As(III). *Nanomaterials* 9, 41. doi:10.3390/nano9010041

Zhou, Y., Jin, P., Zhou, Y., and Zhu, Y. (2018). High-performance Symmetric Supercapacitors Based on Carbon Nanotube/graphite Nanofiber Nanocomposites. *Sci. Rep.* 8, 1–7. doi:10.1038/s41598-018-27460-8

Conflict of Interest: The authors declare that the research was conducted in the absence of any commercial or financial relationships that could be construed as a potential conflict of interest.

Publisher's Note: All claims expressed in this article are solely those of the authors and do not necessarily represent those of their affiliated organizations, or those of the publisher, the editors, and the reviewers. Any product that may be evaluated in this article, or claim that may be made by its manufacturer, is not guaranteed or endorsed by the publisher.